Wang, R. et al. (2013). Nitrogen-doped carbon coated ZrO2 as a support for Pt nanoparticles in the oxygen reduction reaction.
International Journal of Hydrogen Energy, 38: 5783 – 5788
http://dx.doi.org/10.1016/j.ijhydene.2013.03.041

Nitrogen-doped carbon coated ZrO2 as a support for Pt nanoparticles in the oxygen reduction reaction

Rongfang Wang, Keliang Wang, Hui Wang, Qizhao Wang, Julian Key, Vladimir Linkov and Shan Ji

Abstract

A new nitrogen-doped carbon (CN_X) support for Pt electrocatalysts was prepared by carbonizing polypyrrole on the surface of ZrO_2 ($ZrO_2@CN_X$) at high temperature. Well-dispersed Pt nanoparticles were easily formed on the $ZrO_2@CN_X$. The electrocatalyst was characterized by FT-IR, XRD, TEM, XPS. The electrochemical performances indicate that the presence of ZrO_2 modified the electro-structure of Pt on the catalyst surface and that $ZrO_2@CN_X$ had superior oxygen reduction activity compared to a nitrogen-doped carbon coated carbon (C@CNx).

1. Introduction

A main objective in fuel cell research is to develop low-cost, high-performance and durable catalyst materials. Current fuel cell systems have high intrinsic cost and fairly poor durability. Pt and Pt-based alloys are the most commonly used electrocatalysts for proton exchange membrane fuel cells (PEMFC) [1,2]. Due to the global scarcity of Pt and its high cost there is an urgent need to reduce its use, in addition to improving the efficiency of PEMFC. Depositing Pt and Pt-based alloys on a conductive, porous support reduces the cost and improves performance. Interaction between the catalyst and the support can improve catalyst efficiency, decrease catalyst loss, assist in charge transfer, reduce catalyst poisoning (e.g. by CO, S, etc.), and in some cases beneficially affect catalyst particle size [3]. Hence, the choice of support material lies central to the behavior, performance, durability and cost effectiveness of the catalyst and thus the overall fuel cell. Conventionally, highly conductive carbon blacks of turbostratic structures with high surface areas, such as Vulcan XC- 72R, Shawinigan and Black Pearl 2000 are used for catalyst support [3]. However, the corrosion of carbon, resulting from electrochemical oxidation during fuel cell operating conditions is a major contributor to poor durability [3]. Recently, improving the performance of carbonaceous supports and exploring novel non-carbonaceous electrocatalyst support materials have become active research areas [4e7].

In recent years, the use of metal oxides as electrocatalyst supports has been explored to reduce the cost and increase the durability of fuel cells. Metal oxides such as Ti_4O_7 [8], WO_X [9], Fe_3O_4 [10], ZrO_2 [7] and SnO_2 [11] with high surface area, mechanical strength and thermal stability have already proven promising support materials for PEMFC. Among these oxides, ZrO_2, used as a membrane electrode anode (MEA) supporting Pt, has shown comparable performance to MEAs of commercial Pt/C. However, the MEA performance of Pt/ZrO_2 with Nafion was lower than that of conventional Pt/C due to low electric conductivity of Pt/ZrO_2. Therefore, enhancement the ZrO_2 support's electric conductivity forms a goal of interest, i.e. to produce a potentially low-cost high-performance catalyst.

Carbon coating provides an effective method to enhance the electric conductivity of oxides. It is also well known that the nitrogen-doped carbon possesses n-type or metallic behavior and show higher electron mobility than conventional carbon [12]. In this study, a method was developed to form a highly conductive nitrogen-doped carbon layer on the surface of ZrO_2 ($ZrO_2@CN_X$), on to which Pt nanoparticles were deposited to form $Pt/ZrO_2@CN_X$. The $Pt/ZrO_2@CN_X$ catalyst was found to exhibit high electrocatalytic activity for the oxygen reduction reaction (ORR).

2. Experimental

Nitrogen-doped carbon was formed on the surface of ZrO_2 by polymerization of pyrrole (PPy) in a solution containing $(NH_4)_2S_2O_8$ as oxidant. The detailed procedure was as follows: 100 mL of deionized water, 2 g of sodium dodecylbenzene-sulphoate and 1 g of ZrO_2 were added to a flask with stirring under nitrogen atmosphere. When a homogeneous suspension was formed, 0.5 mL of pyrrole was slowly added to the above solution. Then, 1.85 g of $(NH_4)_2S_2O_8$ was added dropwise to the solution which was then stirred at 25 ^{o}C for 1 h $ZrO_2@PPy$ powder was recovered by filtering and dried at 60 ^{o} C. To prepare $ZrO_2@CN_X$, $ZrO_2@PPy$ was carbonized at high temperature in an inert gas oven. A 300 mg of $ZrO_2@PPy$ was placed in a quartz tube furnace and then heated to 800 ^{o} C with a heating rate of 5 ^{o} C min^{-1} under N_2 atmosphere and kept at 800 ^{o} C for 2 h. The furnace was cooled to room temperature and a black powder of $ZrO_2@CN_X$ was obtained. For comparison, carbon coated with nitrogen-doped carbon ($C@CN_X$) was also synthesized using the same procedure. Platinum catalysts (loading ca. 20 wt %) supported on $ZrO_2@CN_X$ were prepared by an ethylene glycol (EG) solution method. H_2PtCl_6 (66.4 mg) was dissolved in 30 mL of EG in a flask. The solution was adjusted to pH 10 by adding 5 wt% of KOH/EG solution. The $ZrO_2@CN_X$ black powder was added to the H_2PtCl_6 solution and then heated at 100 ^{o} C for 10 h. The resulting catalyst ($Pt/ ZrO_2@CN_X$) was filtered, washed with ultrapure water, and

dried in a vacuum oven. C@CN_X supported Pt (Pt/C@CN_X) catalyst was synthesized using the same procedure for preparing Pt/ZrO_2@CN_X.

X-Ray Diffraction (XRD) and X-Ray Photoelectron Spectroscopy (XPS) spectra were generated by a Shimadzu XD-3A (Japan) goniometer with Cu Ka radiation (40 kV, 30 mA) and a PHI-5702 multifunctional X-ray photoelectron spectrometer (American), respectively. Transmission electron microscopy (TEM) measurements were carried out using a JEM-2010 Electron Microscope (Japan) with an acceleration voltage of 200 kV. The chemical composition of the samples was determined using energy dispersive X-ray analysis (EDX) technique coupled to TEM.

The electrochemical measurements of catalysts were carried out using an Autolab electrochemical work station (PGSTAT128N, Eco Chemie, The Netherlands). A conventional three-electrode electrochemical cell was used comprising a platinum wire as the counter electrode, an Ag/AgCl (KCl 3 M) electrode as the reference electrode, and a glass carbon electrode (5 mm in diameter) as the working electrode. All potentials are quoted with respect to the reversible hydrogen electrode (RHE). The thin film electrode was prepared as follows: 5 mg of catalyst was dispersed ultrasonically in 1 mL of Nafion/ethanol (0.25% Nafion). A 8 mL of the dispersion was transferred onto the glassy carbon disc using a pipette, and then dried in air to form the catalyst layer. Before each measurement, the solution was purged with high-purity N_2 (for oxygen-free solutions) or O_2 gas (for oxygen-saturated solutions) for at least 30 min.

3. Results and discussion

Fig. 1 shows the FT-IR spectra of ZrO_2, C@PPy, C@CN_X, ZrO_2@PPy and ZrO_2@CN_X recorded from 4000 to 400 cm^{-1}. In the spectra of these samples, the band at 1400 cm^{-1} is attributed to the C]C stretch vibration, and the bands at 2850 cm^{-1} are assigned to the CeH stretching vibration. In the all samples containing PPy and CN_X, the bands at 1457 cm^{-1} and 3400 cm^{-1}, which are assigned to the CeN stretching vibration and NeH stretching vibration, respectively, are clearly presented in the FT-IR spectra [13]. After carbonization, the CeH stretching bands at 2850 cm^{-1} were absent in the FT-IR spectra of C@CN_X and ZrO_2@CN_X, which indicated that the PPy was completely carbonized after the high temperature treatment. Compared to the FT-IR spectrum of ZrO_2, the FT-IR spectra of ZrO_2@PPy and ZrO_2@CN_X with strong attenuation of the peaks suggest that ZrO_2 particles were completely coated by PPy and CN_X.

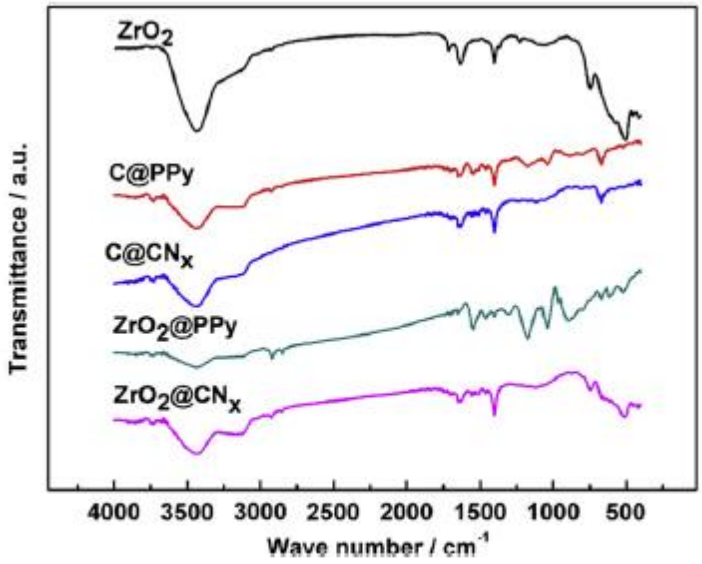

Fig. 1 – FT-IR spectra of ZrO_2, C@PPy, C@CN_x, ZrO_2@PPy and ZrO_2@CN_x.

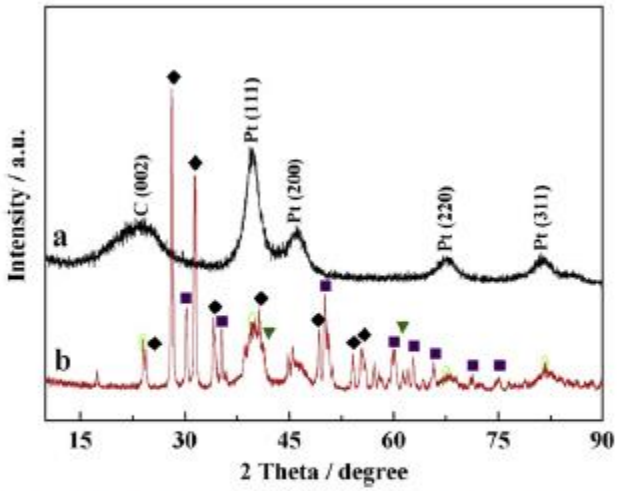

Fig. 2 – XRD patterns of (a) Pt/C@CN_x and (b) Pt/ZrO_2@CN_x, ((◆) ZrO_2 monoclinic, (■) ZrO_2 tetragonal, (▼) ZrO_2 cubic).

XRD patterns in Fig. 2 show the crystalline structure of Pt/ C@CN_X and Pt/ZrO_2@CN_X. The characteristic peaks of mono-clinic ZrO_2 (2q at 24.5^0, 28.2^0, 31.5^0, 34.2^0, 40.8^0, 49.3^0, 54.1^0, 55.4^0) and tetragonal ZrO_2 (2q at 30.1^0, 35.3^0, 50.2^0, 60.1^0, 63.0^0, 65.8^0, 71.2^0, 75.2^0) are clearly shown in the XRD pattern of Pt/ ZrO_2@CN_X [14]. Two small peaks pertaining to cubic ZrO_2 are also present. These results indicate that the commercial ZrO_2 particles form a mixture of mainly monoclinic ZrO_2 and tetragonal ZrO_2 with a small amount of cubic ZrO_2. After CN_X was formed and Pt nanoparticles were deposited on the surface of the ZrO_2 particles, the characteristic peaks of crystalline Pt at 2q ¼ 39.7^0, 46.3^0, 67.6^0,

81.4° (JCPDS, No. 04-0802), which are attributed to the (1 1 1), (2 0 0), (2 2 0), (3 1 1) crystal planes of face-centrered cubic (fcc) Pt, respectively, became clearly present in the XRD pattern [15]. The absence of a diffraction peak related to crystalline carbon indicates that the CN_X formed by carbonization of PPy was amorphous. In the XRD pattern of Pt/C@CN_X, there is a broad peak at 2q ¼ 25° assigned to the amorphous carbon materials, which further indicates that the CN_X synthesized by carbonizing PPy at high temperature formed amorphous structure. The characteristic peaks of crystalline Pt pertaining to the Pt (111), (200), (220) and (311) planes are also clearly observed in the XRD pattern of Pt/ C@CN_X.

TEM images in Fig. 3 show that Pt nanoparticles were well dispersed on the surface of C@CN_X and ZrO_2@CN_X supports. The particle size distributions, insert (a) Pt/C@CN_X and insert (b) Pt/ZrO_2@CN_X, show that the average size of Pt nano-particles on their respective surfaces of was 5.0 and 5.9 nm, respectively. A uniform C@CN_X support is observed in the magnified TEM image (Fig. 3c). EDX spectrum of Pt/C@CN_X is presented as the inset in Fig. 3c, where the presence of C, N, O, and Pt elements are identified. As shown in Fig. 3d, ZrO_2 particles were completely covered by CN_X formed during the carbonization of Ppy, The lattice of Pt and ZrO_2 are clearly shown in Fig. 3d, while the lattice of CN_X is not observed, which further indicates that the CN_X formed on the surface of ZrO2 is amorphous. The presence of C, N, O, Zr and Pt are confirmed by the inset of Fig. 3d.

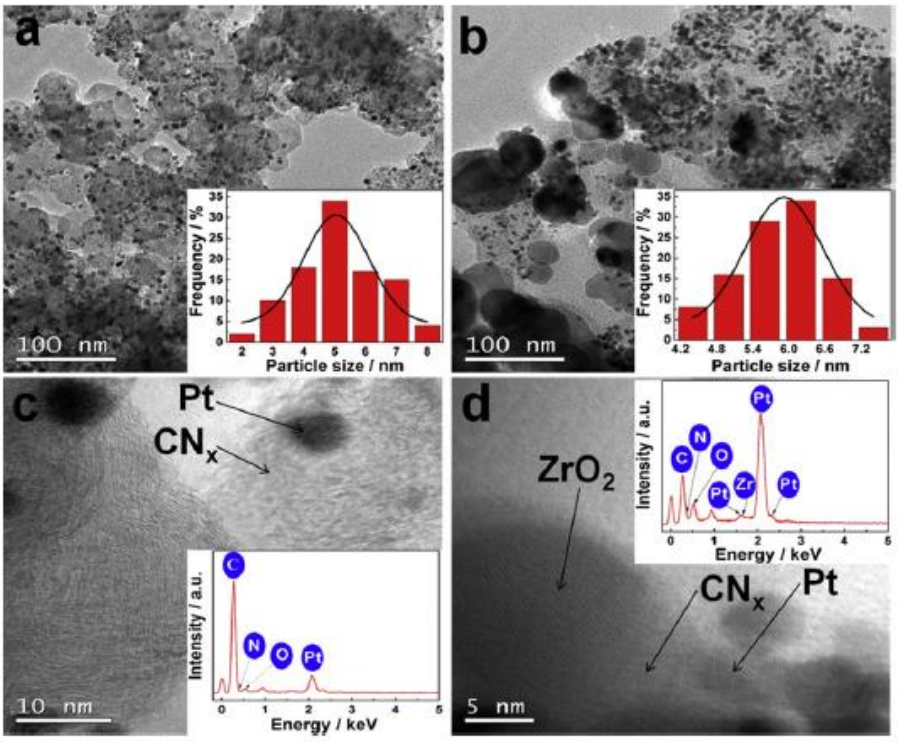

Fig. 3 – TEM images of (a) Pt/C@CN_x and (b) Pt/ZrO_2@CN_x. The particle size distributions of Pt/C@CN_x and (b) Pt/ZrO_2@CN_x are inserted in a and b. The EDX spectrum of Pt/C@CN_x and (b) Pt/ZrO_2@CN_x are inserted in c and d.

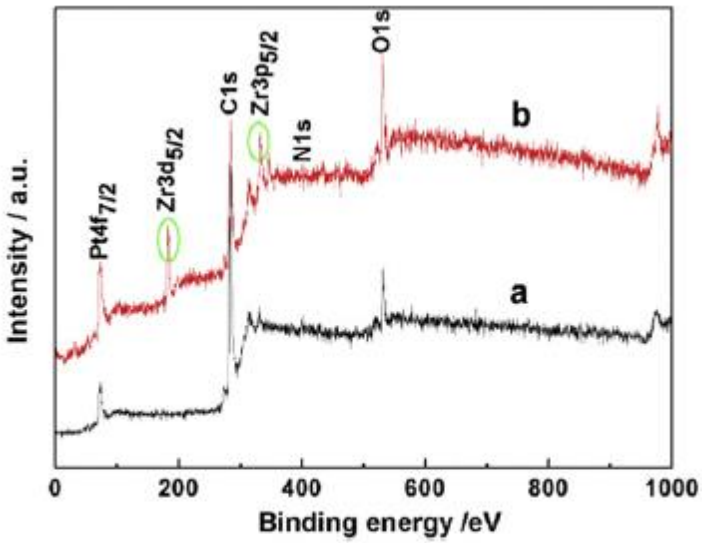

Fig. 4 – XPS spectrum of (a) Pt/C@CN_x and (b) Pt/ZrO_2@CN_x.

Fig. 4 shows the survey XPS spectra of Pt/C@CN_X and Pt/ ZrO_2@CN_X, in which elements of Pt, C, Zr, O and N are detected in the Pt/ZrO_2@CN_X catalyst and Pt, C, O and N are found in the Pt/C@CN_X catalyst. These results confirm the presence of the N element in both catalysts after carbonization of PPy. XPS also provides an efficient way to study the surface oxidation states. As shown in Fig. 5, two peaks in

the Pt 4f binding energy region of Pt/C@CN_X and Pt/ZrO_2@CN_X are observed at (70.6 eV, 73.9 eV) for Pt/C@CN_X and (70.7 eV, 74.2 eV) for Pt/ZrO_2@CN_X, which are attributed to $4f_{7/2}$ and $4f_{5/2}$ of metallic Pt, respectively. Compared with the XPS of Pt/C@CN_X, a clear shift to higher energy region of the Pt 4f peak in the XPS spectrum of Pt/ZrO_2@CN_X has been observed and results from the electronic effect on Pt due to the interaction between Pt and support [16]. To evaluate the surface oxidation states of Pt, the Pt 4f spectra were de-convoluted into three doublets which are assigned to the different oxidation states of Pt. The most intense doublet (around 71 eV and 74 eV) is assigned to metallic Pt. The second doublets (around 71.5 eV and 75 eV), can be attributed to the Pt (II) chemical state, i.e. PtO and $Pt(OH)_2$ [17]. The weakest doublet of Pt at even higher binding energies (around 73.3 eV and 76.3 eV) indicates Pt (IV) in PtO_2 (IV) [18] species existing on the surface of both catalysts. Since the amount of Pt species are related to the relative intensities of these three peaks, the amount of each Pt oxidation states can be calculated from XPS results. The results show that the percentages of each Pt oxidation state for Pt/C@CN_X are Pt(0) 44%, PtO/$Pt(OH)_2$(II) 39%, PtO_2(IV) 17%, and for Pt/ZrO_2@CN_X are Pt(0) 39%, PtO/$Pt(OH)_2$(II) 34%, PtO_2(IV) 27%.

It has been reported that there are four types of nitrogen species found in carbon-based materials such as coal and char [19]. These comprise pyridinic-N (398.6 ± 0.3 eV), pyrrolic-N (400.5 ± 0.3 eV), quaternary nitrogen (401.3 ± 0.3 eV) and pyridinic-$N^{+}eO^{-}$ (402e405 eV). As shown in Fig. 6, there are four peaks in the N 1*s* spectra for both Pt/C@CN_X and Pt/ ZrO_2@CN_X catalysts. It should be noticed that pyridinic-N, which provides one *p*-electron to the aromatic p-systems and has a pair of electrons in the plane of the carbon matrix, can increase the electron-donor property of the catalyst. Pyridinic-N can thus weaken the bond of OeO via bonding with nitrogen or the carbon atom adjacent to it, and further facilitate the oxygen reduction. The pyridinic-N is usually located on the edge of carbon plane and carbon vacancy. In Fig. 6a and b the integrated area ratio of pyridinic-N increased when ZrO_2@CN_X was used as support.

The oxidation state of ZrO_2 is shown in the XPS results in Fig. 7. Two Zr 3d peaks were observed at the binding energies of 182.4 eV and 184.5 eV, which are attributed to ZrO_2 [20]. The result indicates that the oxidation state of ZrO_2 did not change after CN_X was deposited on its surface.

The cyclic voltammetry (CV) results of Pt/C@CN_X and Pt/ ZrO_2@CN_X in 0.5 M H_2SO_4 electrolyte between 0 and 1.2 V -1 (versus RHE) with a scanning rate of 50 mV s , are shown in Fig. 8. Typical CV curves of Pt are observed for both electro-catalysts, i.e. hydrogen adsorption/desorption peaks in the low potential region, oxide formation/stripping wave/peak in the high potential region, and a flat double layer in between. In the potential range from 0 to 0.2 V, three hydrogen desorption

peaks are observed at about 0.01, 0.1, 0.18 V, which correspond to the catalytic effects of Pt (111), Pt (110), Pt (100) planes, on the sample of $Pt/ZrO_2@CN_X$. These three desorption peaks on the sample of $Pt/C@CN_X$ are not as clear as those on $Pt/ZrO_2@CN_X$. The CV curve of $Pt/ZrO_2@CN_X$ also shows two hydrogen absorption peaks, which are absent on $Pt/C@CN_X$. The results suggest that the crystallinity of Pt nanoparticles on the support of $ZrO_2@CN_X$ is higher than that on $C@CN_X$, and thus lead to an enhancement of the ORR kinetics [21]. The ORR polarization curves of $Pt/ZrO_2@CN_X$ and $Pt/C@CN_X$ catalysts in oxygen-saturated 0.5 M H_2SO_4 using a rotating disk electrode at 1600 rpm, Fig. 9.

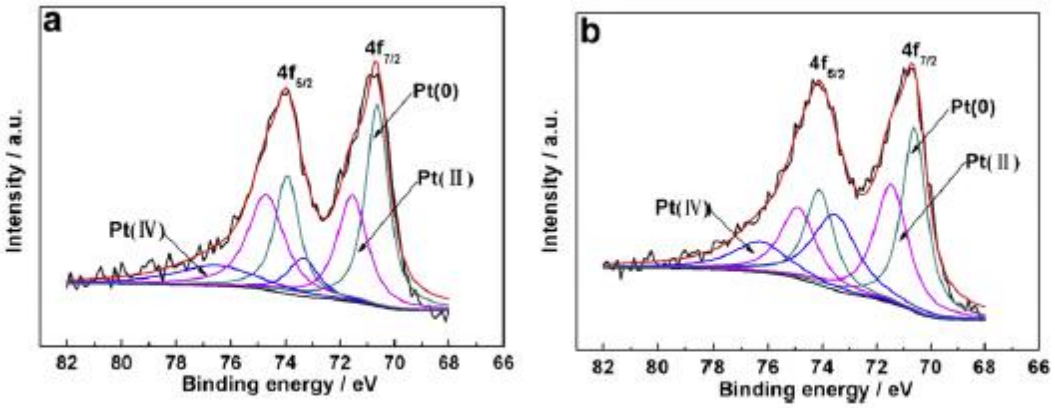

Fig. 5 – XPS spectra of Pt 4f region for the (a) $Pt/C@CN_x$ and (b) $Pt/ZrO_2@CN_x$.

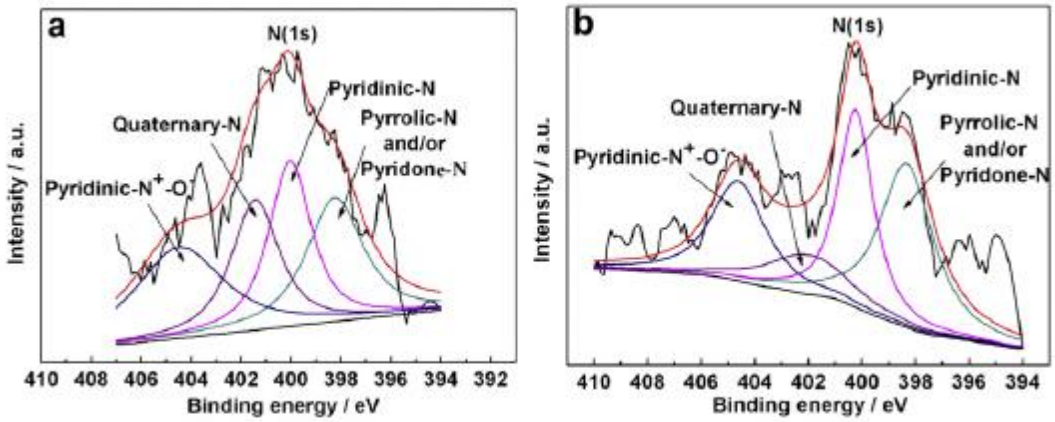

Fig. 6 – XPS spectra of N 1s region for the (a) $Pt/C@CN_x$ and $Pt/ZrO_2@CN_x$.

Here, both the onset and peak potential of $Pt/ZrO_2@CN_X$ catalyst shift to a more positive position. The half-wave potentials of $Pt/ZrO_2@CN_X$ and $Pt/C@CN_X$ catalysts were 0.77 V and 0.73 V, respectively. The half-wave potentials of $Pt/ZrO_2@CN_X$ is higher than that of $Pt/C@CN_X$ catalyst, showing that the $Pt/ZrO_2@CN_X$ is more active towards ORR, apparently due to the ZrO_2 support.

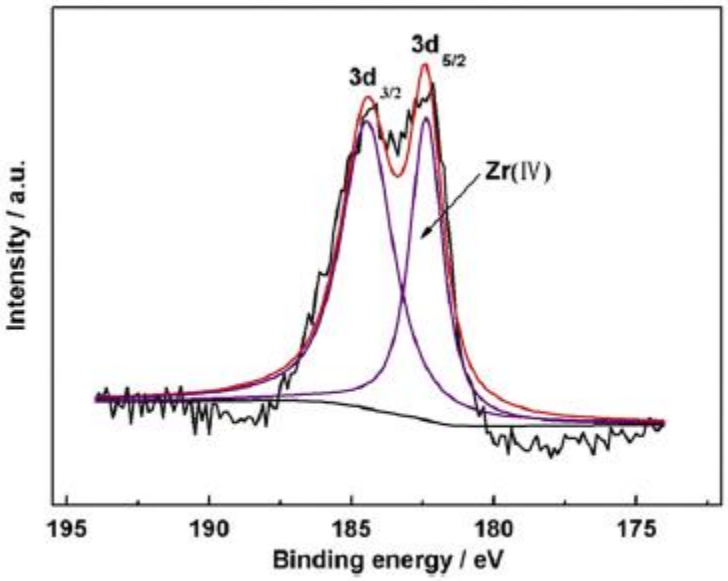

Fig. 7 – XPS spectra of Zr 3d region for the $Pt/ZrO_2@CN_x$.

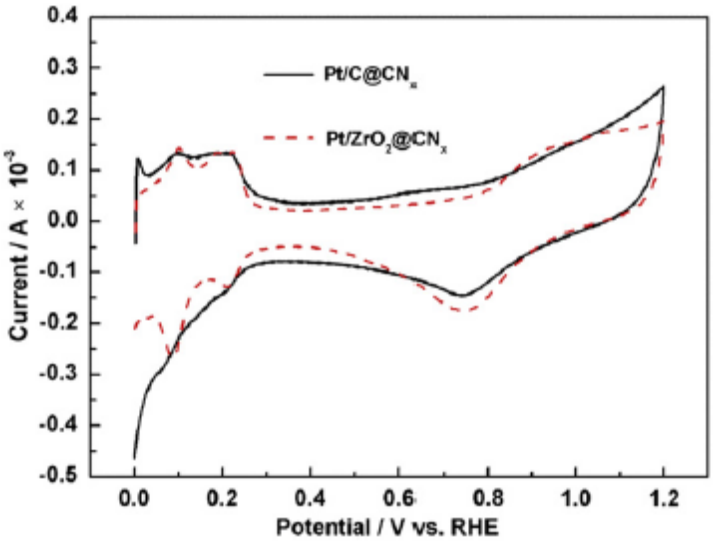

Fig. 8 – Cyclic voltammograms of $Pt/C@CN_x$ and $Pt/ZrO_2@CN_x$ electrocatalysts in 0.5 M H_2SO_4 at 50 mV s^{-1} at room temperature.

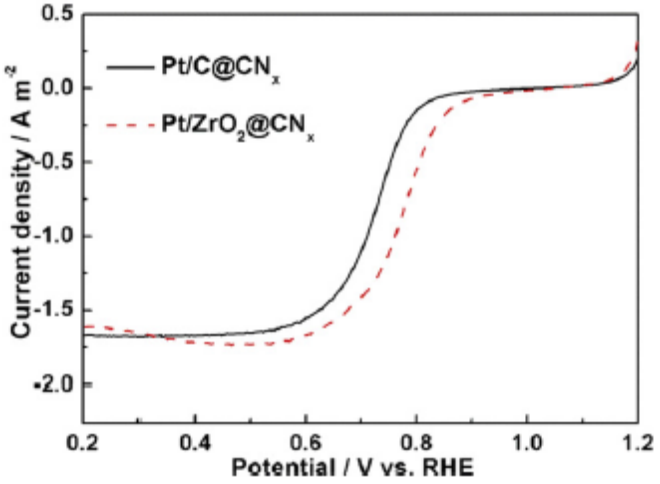

Fig. 9 – Polarization curves of ORR on Pt/ZrO_2@CN_x and Pt/C@CN_x catalysts in oxygen-saturated 0.5 M H_2SO_4; rotation rates 1600 rpm, 30 °C, scan rate: 5 mV s^{-1}.

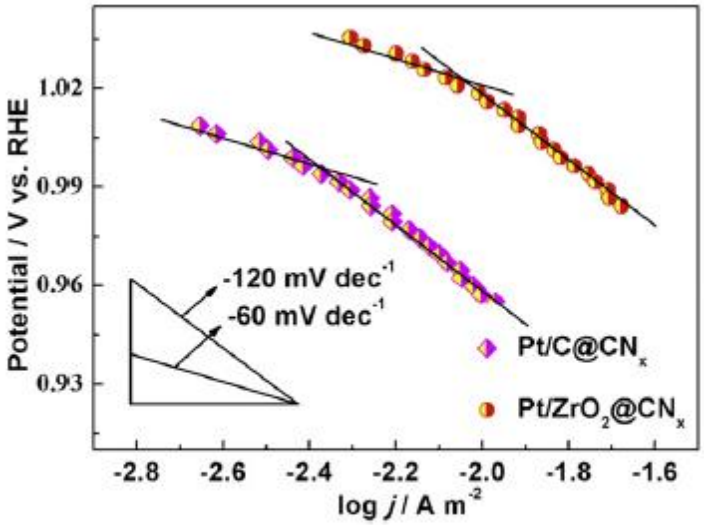

Fig. 10 – Tafel plots for ORR on Pt/C@CN_x and Pt/ZrO_2@CN_x; 30 °C, scan rate: 5 mV s^{-1}, rotation rate: 1600 rpm.

Tafel plots for the kinetic current density normalized to the electrochemical active surface are presented in Fig. 10. The Tafel lines of the Pt/ZrO_2@CN_X catalyst clearly moved to a higher potential region, compared to the Pt/C@CN_X catalyst, suggesting that the Pt/ZrO_2@CN_X catalyst had a higher kinetic ORR activity. Both Pt/C@CN_X and Pt/ZrO_2@CN_X show two Tafel regions with slopes of -60 mV dec^{-1} at the low current region, and -120 mV dec^{-1} at the high current region, which indicate that the ORR on both catalysts follows the same mechanism as in Pt/C catalysts [22]. Therefore the rate determining steps for ORR on ZrO_2@CN_X support material appear to be the same as on carbon.

4. Conclusions

Forming nitrogen-doped carbon on the surface of metal oxides, ZrO_2, via carbonization at high temperature provides a useful method for synthesizing support of electrocatalysts. Well-dispersed Pt nanoparticles were successfully synthesized on the surface of $ZrO_2@CN_X$ supports. The electrochemical data for ORR demonstrate that $Pt/ZrO_2@CN_X$ is more active than $Pt/C@CN_X$ due to the ZrO_2 support, and follows the same mechanism as Pt/C catalyst. Further work is underway to determine how ZrO_2 affects the ORR activity and its longterm stability.

Acknowledgments

The authors would like to thank the National Natural Science Foundation of China (21163018, 51262028) and the National Science Foundation for Post-doctoral Scientists of China (20110490847, 2012T50554) for financially supporting this work.

References

[1] Wang R, Li H, Ji S, Wang H, Lei Z. Pt decorating of PdNi/C as electrocatalysts for oxygen reduction. Electrochim Acta 2010;55:1519e22.
[2] Xia BY, Wang JN, Wang XX. Synthesis and application of Pt nanocrystals with controlled crystallographic planes. J Phys Chem C 2009;113:18115e20.
[3] Sharma S, Pollet BG. Support materials for PEMFC and DMFC electrocatalysts e a review. J Power Sources 2012;208:96e119.
[4] Wang YJ, Wilkinson DP, Zhang J. Noncarbon support materials for polymer electrolyte membrane fuel cell electrocatalysts. Chem Rev 2011;111:7625e51.
[5] Wang KL, Wang H, Pasupathi S, Linkov V, Ji S, Wang RF. Palygorskite promoted PtSn/carbon catalysts and their intrinsic catalytic activity for ethanol oxidation. Electrochim Acta 2012;70:394e401.
[6] Jia J, Wang R, Wang H, Ji S, Key J, Linkov V, et al. A novel structural design of CNx-Fe_3O_4 as support to immobilize Pd for catalytic oxidation of formic acid. Catal Commun 2011;16:60e3.
[7] Suzuki Y, Ishihara A, Mitsushima S, kamiya N, Ota K-i. Sulfated-zirconia as a support of Pt catalyst for polymer electrolyte fuel cells. Electrochem Solid-state Lett 2007;10:B105e7.
[8] Chen G, Bare SR, Mallouk TE. Development of supported bifunctional electrocatalysts for unitized regenerative fuel cells. J Electrochem Soc 2002;149:A1092e9.
[9] Sun Z, Chiu HC, Tseung ACC. Oxygen reduction on teflon bonded Pt/WO_3/C electrode in sulfuric acid. Electrochem Solid-state Lett 2001;4:E9e12.
[10] Wang C, Daimon H, Sun S. Dumbbell-like Pt-Fe_3O_4 nanoparticles and their enhanced catalysis for oxygen reduction reaction. Nano Lett 2009;9:1493e6.
[11] Matsui T, okanishi T, Fujiwara K, Tsutsui K, Kikuchi R, Takeguchi T, et al. Effect of reduction-oxidation treatment on the catalytic activity over tin oxide supported platinum catalysts. Sci Technol Adv Mat 2006;7:524e30.
[12] Xiao K, Liu Y, Pa Hu, Yu G, Sun Y, Zhu D. n-Type field-effect transistors made of an individual nitrogen-doped multiwalled carbon nanotube. J Am Chem Soc 2005;127:8614e7.
[13] Jeyabharathi C, Venkateshkumar P, Mathiyarasu J, Phani KLN. Carbon-supported palladium-polypyrrole nanocomposite for oxygen reduction and its tolerance to methanol. J Electrochem Soc 2010;157:B1740e5.
[14] Reddy GK, Loridant S, Takahashi A, Deliche` re P, Reddy BM. Reforming of methane with carbon dioxide over Pt/ZrO_2/SiO_2 catalysts e effect of zirconia to silica ratio. Appl Catal A: Gen 2010;389:92e100.
[15] Li Y, Gao W, Ci L, Wang C, Ajayan PM. Catalytic performance of Pt nanoparticles on reduced graphene oxide for methanol electro-oxidation. Carbon 2010;48:1124e30.
[16] Su F, Tian Z, Poh CK, Wang Z, Lim SH, Liu Z, et al. Pt nanoparticles supported on nitrogen-doped porous carbon nanospheres as an electrocatalyst for fuel cells. Chem Mater 2009;22:832e9.

[17] Sheng W, Chen S, Vescovo E, Shao-Horn Y. Size influence on the oxygen reduction reaction activity and instability of supported Pt nanoparticles. J Electrochem Soc 2012;159:B96e103.
[18] Roth C, Goetz M, Fuess H. Synthesis and characterization of carbon-supported PteRueWO catalysts by spectroscopic and diffraction methods. J Appl Electrochem 2001;31:793e8.
[19] Pels JR, Kapteijn F, Moulijn JA, Zhu Q, Thomas KM. Evolution of nitrogen functionalities in carbonaceous materials during pyrolysis. Carbon 1995;33:1641e53.
[20] Liu H, Liu G, Shi X. N/Zr-codoped TiO_2 nanotube arrays: fabrication, characterization, and enhanced photocatalytic activity. Colloids Surf A Physicochem Eng Asp 2010;363:35e40.
[21] Santos LGRA, Freitas KS, Ticianelli EA. Heat treatment effect of PteV/C and Pt/C on the kinetics of the oxygen reduction reaction in acid media. Electrochim Acta 2009;54:5246e51.
[22] Wang R, Jia J, Li H, Li X, Wang H, Chang Y, et al. Nitrogen-doped carbon coated palygorskite as an efficient electrocatalyst support for oxygen reduction reaction. Electrochim Acta 2011;56:4526e31.